Enhanced finite elements for the simulations of structures with embedded anchors

Francesco Riccardi, Cédric Giry, Fabrice Gatuingt

10^{th} International Conference on Fracture Mechanics of Concrete and Concrete Structures
FraMCoS-X
G. Pijaudier-Cabot, P. Grassl and C. La Borderie (Eds)

ENHANCED FINITE ELEMENTS FOR THE SIMULATIONS OF STRUCTURES WITH EMBEDDED ANCHORS

Francesco Riccardi[*], **Cédric Giry**[†], **Fabrice Gatuingt**[‡]

[*]LMT, ENS Paris-Saclay, CNRS, Université Paris-Saclay
61 Avenue du Président Wilson, F-94235 Cachan, France
e-mail: francesco.riccardi@ens-paris-saclay.fr

[†]LMT, ENS Paris-Saclay, CNRS, Université Paris-Saclay
61 Avenue du Président Wilson, F-94235 Cachan, France
e-mail: cedric.giry@ens-paris-sacaly.fr

[‡]LMT, ENS Paris-Saclay, CNRS, Université Paris-Saclay
61 Avenue du Président Wilson, F-94235 Cachan, France
e-mail: fabrice.gatuingt@ens-paris-saclay.fr

Key words: FRP, Reinforced Concrete, Anchors, Interface

Abstract. The embedding of anchoring systems in the retrofitting of Reinforced Concrete (RC) structures by means of Fiber Reinforced Polymers (FRP) often implies local failure modes associated to high stress concentrations. In order to account for such mechanical behaviours in standard finite element computations, an explicit representation of interfaces is required. This strategy presents, however, several limitations in terms of computational cost and mesh-related issues. On the other hand, implicit models may not be sufficiently accurate in order to reproduce the aforementioned localized phenomena. Specific finite elements for the simulation of pull-out mechanisms are here presented. The presence of interfaces is taken into account by enriching the displacement approximation by means of additional unknowns defined at the element level. Static-condensation, therefore, allows preserving the structure of the finite element procedure and limiting the computational effort.

1 INTRODUCTION

The good performances of FRP materials in enhancing the bearing capacity and ductility of RC structures have been well-acknowledged by extensive experimental campaigns during the last decades. One of the main issues related to this technology is, however, the stress transfert between concrete and reinforcements, in particular under flexural loading conditions. Suitable anchoring systems are therefore required [1–4]. These often consist in composite meshes which are glued through drilled holes to concrete. The latter are highly recommended especially in case of joints between vertical and horizontal elements, where non-anchored FRP strips fail in ensuring the load transfer, as pointed out in [5, 6]. The introduction of anchors mobilizes the tensile resistance of the reinforcement with shear stresses developing at the interface between FRP and concrete. The overall failure is then associated in most cases with the anchor pull-out or its rupture, where debonding is often due to cracking of nearby concrete [4–6]. The choice of an appropriate numerical model for simulating the bending behaviour of RC structures strenghtened with FRP must then take into account the aforementioned observations. In order to deal with full-scale sim-

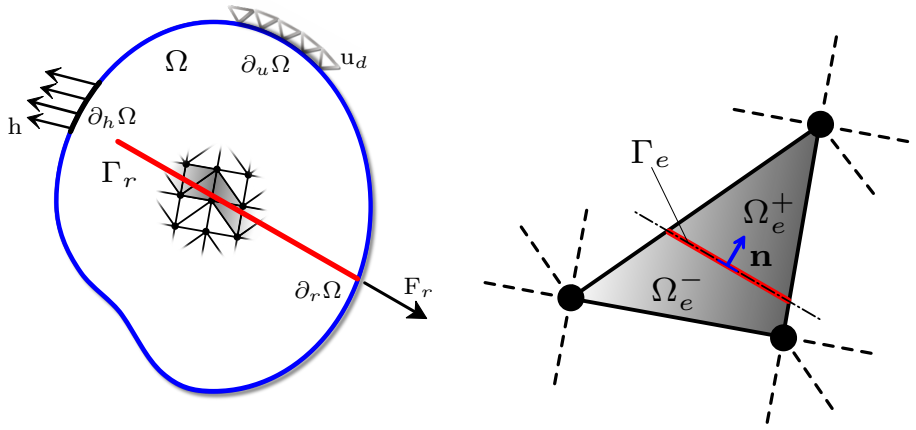

(a) (b)

Figure 1: 2D body with an embedded reinforcement.

ulations, concrete and reinforcements are often discretized separately. Kinematic relations are then written between DOFs associated to each material and the interfacial behaviour is computed in an averaged sense. In order to model bond-slip behaviours, interface finite elements can be added to such macroscopic representation [7,8]. A different strategy is to enrich the finite element approximation without resorting to remeshing techniques, as is done in the framework of the Extended Finite Element Method (X-FEM) [9–11] and in the Embedded Finite Element Method (E-FEM) [12–14]. In this paper, a finite element model with enhanced kinematics for the simulation of structures with embedded anchors is presented. An elemental enrichment is added to the macroscopic model in order to catch the interfacial behaviour associated with local shear stresses. The proposed formulation is validated at the element level for different configurations and compared to standard finite element simulations.

2 NUMERICAL MODEL

2.1 Spatial discretization

Let us consider a 2D body Ω and its boundary $\partial\Omega$, crossed by a reinforcement r whose axis is denoted by Γ_r (see Figure 1a). Dirichlet and Neumann boundary conditions are imposed on portions $\partial_u\Omega \subset \partial\Omega$ and $\partial_t\Omega \subset \partial\Omega$, respectively, such that $\partial\Omega = \overline{\partial_u\Omega \cup \partial_t\Omega}$ and $\partial_u\Omega \cap \partial_t\Omega = \emptyset$. We also assume that there exists a part of the boundary $\partial_r\Omega \subset \partial_t\Omega$ where the resultant $\mathbf{F}_r$ acts. We indicate then with Ω_h the spatial discretization of Ω and $\Omega_h^r = \bigcup_{e=1}^{N_e^r} \Omega_e$ the set of elements crossed by Γ_r.

2.2 Finite element approximation

Each elementary domain $\Omega_e \in \Omega_h^r$, characterized by N nodes, is then decomposed into two subdomains Ω_e^+ and Ω_e^- as shown in Figure 1b. Its kinematics is approximated as follows:

$$\mathbf{u} \approx \mathbf{u}_h = \mathbf{N}\mathbf{d} + \mathbf{N}_r\mathbf{d}_r \tag{1}$$

where $\mathbf{d}$ are the nodal displacements, $\mathbf{d}_r$ the enriching variables defined at the center of gravity of segment Γ_e, $\mathbf{N}$ is the standard shape function matrix and $\mathbf{N}_r$ is defined as:

$$\mathbf{N}_r = \begin{bmatrix} N_r & 0 \\ 0 & N_r \end{bmatrix} \tag{2}$$

Function N_r is chosen such that the kinematic boundary conditions can still be expressed in terms of the sole nodal displacements, i.e. by imposing:

$$N_r(\mathbf{x}_j) = \mathbf{0} \quad , \quad \forall \mathbf{x}_j \in \Omega_h^r \tag{3}$$

where $\mathbf{x}_j$ denotes the coordinates of node j. In addition, the compatible strain field reads:

$$\boldsymbol{\epsilon} \approx \boldsymbol{\epsilon}_h = \mathbf{B}\mathbf{d} + \mathbf{G}_r\mathbf{d}_r \tag{4}$$

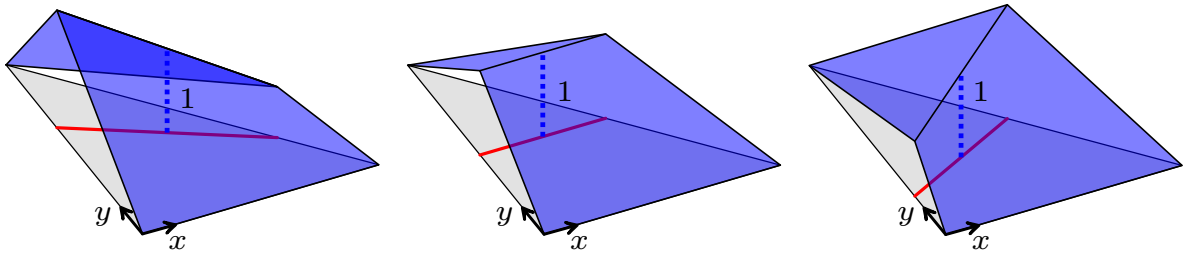

(a) (b) (c)

Figure 2: Function N_r in case of CST triangles for different anchor inclinations: (a) $\alpha_r = -20°$, (b) $\alpha_r = 0°$, (c) $\alpha_r = 20°$.

where $\mathbf{B} = \mathbf{L}\mathbf{N}$ and $\mathbf{G}_r = \mathbf{L}\mathbf{N}_r$ compute the strain field associated to the nodal and enhanced displacements, respectively.

2.3 Governing equations

Let us consider the case of a single finite element. In absence of body forces, by applying the Principle of Virtual Works (PVW) and following a similar reasoning as for the SKON formulation proposed in the framework of the Embedded Finite Element Method (E-FEM) [13], the governing equations reads:

$$\begin{cases} \displaystyle\int_{\Omega_e} \mathbf{B}^{\mathsf{T}} \boldsymbol{\sigma} \, \mathrm{d}A = \mathbf{F}^e_{ext} & \text{(5a)} \\ \displaystyle\int_{\Omega_e} \mathbf{G}^*_r \boldsymbol{\sigma} \, \mathrm{d}A = \mathbf{F}^e_r & \text{(5b)} \end{cases}$$

with

$$\mathbf{F}^e_{ext} = \int_{\partial_t \Omega_e} \mathbf{N}^{\mathsf{T}} \mathbf{h} \, \mathrm{d}\Gamma \tag{6}$$

where $\boldsymbol{\sigma} = \boldsymbol{\sigma}\left(\mathbf{B}\mathbf{d} + \mathbf{G}_r \mathbf{d}_r\right)$ denotes the stress field and $\mathbf{G}^*_r$ is a matrix satisfying the condition of zero mean, defined as:

$$\mathbf{G}^*_r = \frac{1}{k_+ k_- l_{\Gamma_e}} \left(|\Omega^+_e| \chi_- - |\Omega^-_e| \chi_+ \right) \mathbf{p}^{\mathsf{T}} \tag{7}$$

In expression (7) the following terms appear: χ_+ and χ_-, denoting the characteristic functions of Ω^+_e and Ω^-_e, resepctively; l_{Γ_e}, the length of segment Γ_e; $\mathbf{p}$, the matrix containing the components of the normal $\mathbf{n}$; k_+ and k_-, defined as:

$$k_+ = \frac{|\Omega^+_e|}{l_{\Gamma_e}} \quad , \quad k_- = \frac{|\Omega^-_e|}{l_{\Gamma_e}} \tag{8}$$

Eq. (14a) states the global equilibrium between internal and external forces, whereas Eq. (14b) translates a local equilibrium condition along Γ_e.

2.4 Kinematic enrichment

After introducing the Heaviside function centered on Γ_e defined as:

$$\mathcal{H}_{\Gamma_e}(\mathbf{x}) = \begin{cases} 1, & \mathbf{x} \in \Omega^+_e \\ 0, & \mathbf{x} \in \Omega^-_e \end{cases} \tag{9}$$

in the framework of a pull-out analysis, a possible choice for function N_r is:

$$\begin{aligned} N_r(\mathbf{x}) = \chi_+ \sum_{i=1}^{N} a_i (1 - \mathcal{H}_{\Gamma_e}(\mathbf{x}_i)) N_i(\mathbf{x}) \\ + \chi_- \sum_{i=1}^{N} a_i \mathcal{H}_{\Gamma_e}(\mathbf{x}_i) N_i(\mathbf{x}) \end{aligned} \tag{10}$$

where N_i is the shape function associated to node i and a_i are constants ensuring a C^0-continuity across Γ_e (see Figure 2). By taking into account expression (10), interpolant $\mathbf{N}_r$ can therefore be written in a compact form as:

$$\mathbf{N}_r = \chi_+ \mathbf{N}(\mathbf{I} - \mathbf{H})\mathbf{A} + \chi_- \mathbf{N}\mathbf{H}\mathbf{A} \tag{11}$$

where $\mathbf{I}$ and $\mathbf{H}$ are (2Nx2N) matrices and $\mathbf{A}$ is of dimension (2Nx2). Matrix $\mathbf{G}_r$ assumes then the following expression:

$$\mathbf{G}_r = \chi_+ \mathbf{B}(\mathbf{I} - \mathbf{H})\mathbf{A} + \chi_- \mathbf{B}\mathbf{H}\mathbf{A} \tag{12}$$

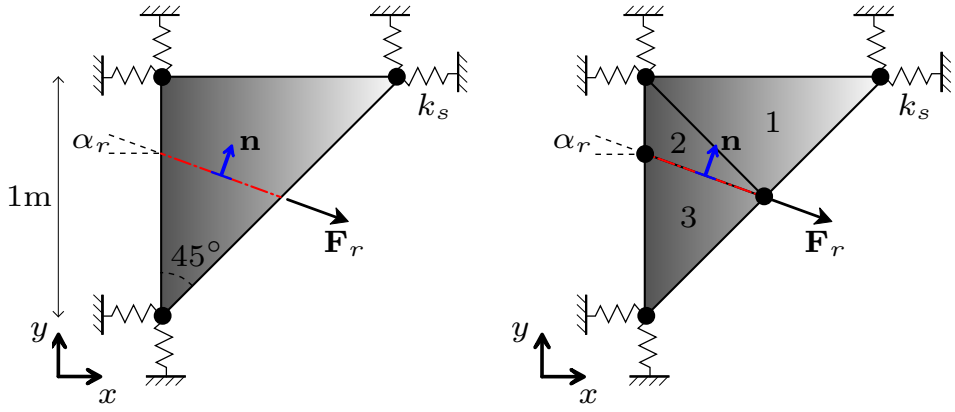

Figure 3: 2D case study: (1) macroscopic model, (2) mesoscopic model.

2.5 Resolution

In case of a linear elastic behaviour, the stress is expressed as:

$$\sigma = \mathbf{D}\boldsymbol{\epsilon} = \mathbf{D}\left(\mathbf{B}\mathbf{d} + \mathbf{G}_r\mathbf{d}_r\right) \tag{13}$$

where $\mathbf{D}$ is the stiffness of the material. Substituing relation (13) into system (5), we obtain:

$$\begin{cases} \mathbf{K}^e_{bb}\mathbf{d} + \mathbf{K}^e_{bg}\mathbf{d}_r = \mathbf{F}^e_{ext} & \text{(14a)} \\ \mathbf{K}_{gb}\mathbf{d} + \mathbf{K}^e_{gg}\mathbf{d}_r = \mathbf{F}^e_r & \text{(14b)} \end{cases}$$

where we have defined the matrices:

$$\begin{aligned} \mathbf{K}^e_{bb} &= \int_{\Omega_e} \mathbf{B}^\mathsf{T}\mathbf{D}\mathbf{B}\,\mathrm{d}A \\ \mathbf{K}^e_{bg} &= \int_{\Omega_e} \mathbf{B}^\mathsf{T}\mathbf{D}\mathbf{G}_r\,\mathrm{d}A \\ \mathbf{K}^e_{gb} &= \int_{\Omega_e} \mathbf{G}^*\mathbf{D}\mathbf{B}\,\mathrm{d}A \\ \mathbf{K}^e_{gg} &= \int_{\Omega_e} \mathbf{G}^*\mathbf{D}\mathbf{G}_r\,\mathrm{d}A \end{aligned} \tag{15}$$

If we collect $\mathbf{d}_r$ from the second equation, we have:

$$\mathbf{d}_r = \left(\mathbf{K}^e_{gg}\right)^{-1}\left(\mathbf{F}^e_r - \mathbf{K}^e_{gb}\mathbf{d}\right) \tag{16}$$

The nodal displacements can therefore be computed by replacing expression (16) into equation (14a) as:

$$\mathbf{d} = \tilde{\mathbf{K}}_e^{-1}\left(\mathbf{F}^e_{ext} - \mathbf{K}^e_{bg}\left(\mathbf{K}^e_{gg}\right)^{-1}\mathbf{F}^e_r\right) \tag{17}$$

where

$$\tilde{\mathbf{K}}_e = \mathbf{K}^e_{bb} - \mathbf{K}^e_{bg}\left(\mathbf{K}^e_{gg}\right)^{-1}\mathbf{K}^e_{gb} \tag{18}$$

is the condensed stiffness matrix.

3 NUMERICAL VALIDATION

3.1 Problem description

Let us consider the case study depicted in Figure 3, where CST elements have been used. The effect of an embedded anchor is here represented by the force $\mathbf{F}_r = F_r\cos\alpha_r\mathbf{i}_x + F_r\sin\alpha_r\mathbf{i}_y$, with $F_r = 10^5\,\mathrm{N}$, applied in the middle of the right side of the structure. Linear springs with stiffness $k_s = 2.36\times10^9\,\frac{\mathrm{N}}{\mathrm{m}}$ are introduced. The material parameters are $E = 30\,\mathrm{GPa}$ and $\nu = 0.2$. Plane stress conditions are assumed for the computations (thickness $t = 0.1\,\mathrm{m}$). The effect of the inclination α_r on the numerical response is studied while keeping the load application point fixed. The enhanced model presented in Section 2 is compared to the reference mesoscopic model counting three finite elements, decomposed into $\Omega^+ = \Omega_1 \cup \Omega_2$ and $\Omega^- \equiv \Omega_3$ (see Figure 3b), and to the single finite element model with standard kinematics and no interface representation.

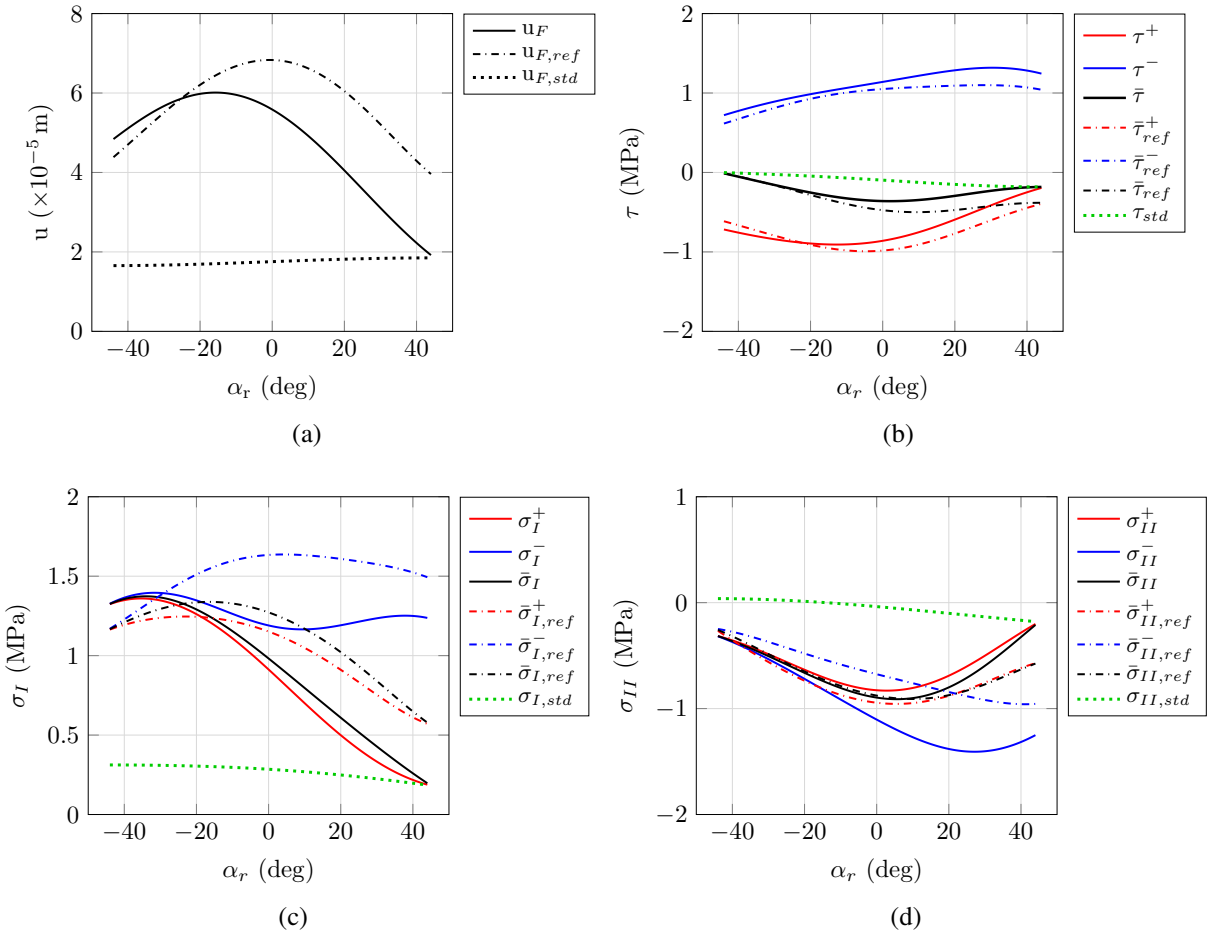

Figure 4: Comparative curves: displacement at load application point (a), local shear stresses (b), maximum principal stresses (c), minimum principal stresses (d).

3.2 Results

The displacement u_F at the load application point, the local shear stress τ, computed as:

$$\tau = (\sigma_y - \sigma_x)\sin\alpha_r\cos\alpha_r + \tau_{xy}\left(\cos^2\alpha_r - \sin^2\alpha_r\right) \tag{19}$$

the principal stresses σ_I and σ_{II} and their directions α_I and α_{II} are compared. The total average $\bar{(\cdot)}$ of quantity $(\cdot)$ is computed as:

$$\bar{(\cdot)} = \frac{1}{|\Omega|}\int_\Omega (\cdot)\,\mathrm{d}A \tag{20}$$

whereas local averages are defined as:

$$\begin{aligned}\bar{(\cdot)}^+ &= \frac{1}{|\Omega^+|}\int_{\Omega^+} (\cdot)\,\mathrm{d}A \\ \bar{(\cdot)}^- &= \frac{1}{|\Omega^-|}\int_{\Omega^-} (\cdot)\,\mathrm{d}A\end{aligned} \tag{21}$$

As can be seen in Figure 4, the enhanced model performs pretty well with respect to the reference simulation, especially in computing local shear stresses (Figure 4b). The evaluation of normal stresses is slightly less precise, but still satisfying (Figures 4c and 4d). On the contrary, it appears that in absence of internal degrees of freedom, standard finite elements are not suitable for evaluating the interfacial stress field induced by pull-out mechanisms. Such behaviour is associated with local shear stresses of opposite sign, whose average value goes to zero as $|\Omega^+| = |\Omega^-|$ (when $\alpha_r \to -45°$). This observation is corroborated by comparing the principal stress directions (Figure 5), for which we have $\bar{\alpha}_i \approx \bar{\alpha}_{i,ref} \approx \alpha_{i,std}$, $\forall\alpha_r$, with $i = I, II$.

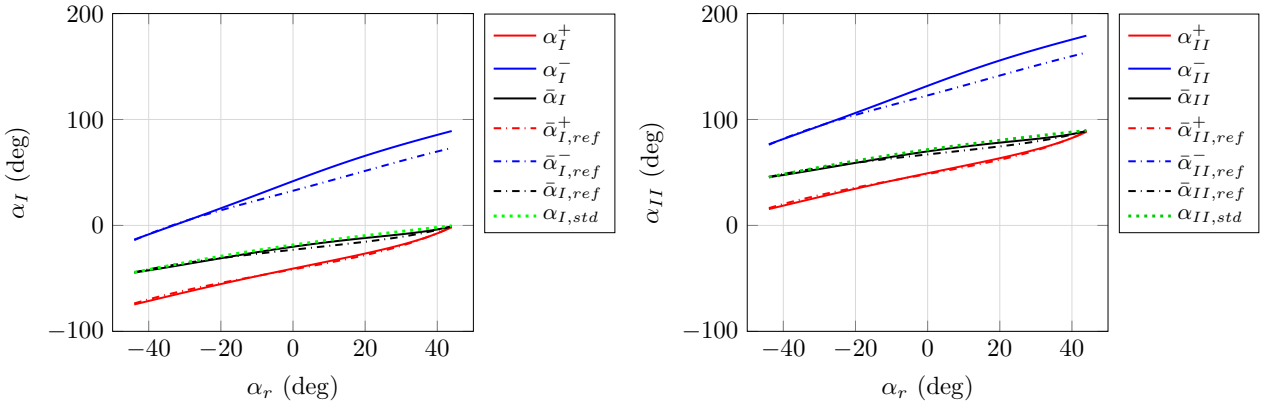

(a) (b)

Figure 5: Comparative curves: maximum principal stress direction (a), minimum principal stress direction (b).

4 CONCLUSIONS

A finite element with enhanced kinematics for the simulation of structures with embedded anchors of arbitrary orientation has been proposed. An enrichment is added to the kinematic approximation for reproducing local mechanism arising along the interface at the additional cost of solving a local equilibrium equation. The proposed model performs well with respect to a full model where the interface is explicity represented, especially in evaluating the shear stresses which are considered to be responsible for the experimentally observed debonding failure modes. Complete structural simulations, including nonlinear material responses, have to be performed in order to fully validate the proposed numerical model.

REFERENCES

[1] R Sadone, M Quiertant, S Chataigner, J Mercier and E Ferrier. 2011. Behavior of an innovative end-anchored externally bonded CFRP strengthening system under low cycle fatigue. In *Advances in FRP Composites in Civil Engineering*, 537–540. Springer, Berlin, Heidelberg.

[2] S T Smith, S Hu, S J Kim and R Seracino. 2011. FRP-strengthened RC slabs anchored with FRP anchors. *Engineering Structures*, 33(4):1075–1087.

[3] S Qazi, L Michel, and E Ferrier. 2013. Mechanical behaviour of slender RC walls under seismic loading strengthened with externally bonded CFRP. *European Journal of Environmental and Civil Engineering*, 17(6):496–506.

[4] T Ozbakkaloglu and M Saatcioglu. 2009. Tensile behavior of FRP anchors in concrete. *Journal of Composites for Construction*, 13(2):453–461.

[5] F Ceroni, M Pecce, S Matthys and L Taerwe. 2008. Debonding strength and anchorage devices for reinforced concrete elements strengthened with FRP sheets. *Composites Part B: Engineering*, 39(3):429–441.

[6] S Qazi, L Michel, and E Ferrier. 2013. Experimental investigation of CFRP anchorage systemsused for strengthening RC joints. *Composite Structures*, 99:453–461.

[7] A Casanova, L Jason, and L Davenne. 2012. Bond slip model for the simulation of reinforced concrete structures. *Engineering Structures*, 39:66–78.

[8] C Mang, L Jason, and L Davenne. 2015. A new bond slip model for reinforced concrete structures: Validation by modelling a

reinforced concrete tie. *Engineering Computations*, 32(7):1934–1958.

[9] T Belytschko and T Black. 1999. Elastic crack growth in finite elements with minimal remeshing. *International journal for numerical methods in engineering*, 45(5):601–620.

[10] N Moës, J Dolbow and T Belytschko. 1999. A finite element method for crack growth without remeshing. *International Journal for Numerical Methods in Engineering*, 46(1):131–150.

[11] J Dolbow, N Moës and T Belytschko. 2000. Discontinuous enrichment in finite elements with a partition of unity method. *Finite Elements in Analysis and Design*, 36(3):235–260.

[12] Armero F, Garikipati K. 1996. An analysis of strong discontinuities in multiplicative finite strain plasticity and their relation with the numerical simulation of strain localization in solids. *International Journal of Solids and Structures*, 133(20):2863–85.

[13] M Jirásek. 2000. Comparative study on finite elements with embedded discontinuities. *Computer Methods in Applied Mechanics and Engineering*, 188(1):307–330.

[14] J Oliver, A E Huespe, and P J Sánchez. 2000. A comparative study on finite elements for capturing strong discontinuities: E-FEM vs X-FEM. *Computer Methods in Applied Mechanics and Engineering*, 195(37–40):4732–4752.